Experimental investigation on beam smoothing by combined spectral dispersion and lens array technology

Youen Jiang (姜有恩)[*], **Shenlei Zhou (周申蕾), Rong Wu (邬 融),**
Jinghui Li (李菁辉), Xuechun Li (李学春), and Zunqi Lin (林尊琪)

National Laboratory of High Power Laser Physics, Shanghai Institute of Optics and Fine Mechanics,
Chinese Academy of Sciences, Shanghai 201800, China
[*]*Corresponding author: joyen@siom.ac.cn*

The experimental performance of beam smoothing by combined one-dimensional (1D) spectral dispersion and lens array (LA) technology is presented, as applied in the ninth beam of SG-II. Using 3ω spectral dispersion with a bandwidth of 270 GHz and a line dispersion that is 24.9 times the beam's diffraction-limited width decreases the focal spot non-uniformity of 80% energy concentration from 46% to 17%. The multiple-beam interference properties of the LA are theoretically and experimentally validated by spatial power spectral density analysis. Peak–spectra suppression ratios of 20 and 10 dB are achieved in the dispersion and orthogonal directions, respectively.

OCIS codes: 140.3580, 140.3610, 350.2660, 030.6140, 030.6600
doi: 10.3788/COL201311.081404.

In inertial confinement fusion experiments, uniform irradiation on a target is an essential condition for successful ignition. To achieve high irradiation uniformity, a combination of beam-smoothing techniques is employed in high-power solid-state laser systems, such as Omega[1] and National Ignition Facility[2]. A focal spot is enlarged and shaped by spatial beam conditioning technologies, including random phase plates (RPP), kinoform phase plates (KPP), distribution phase plate (DPP)[3], continuous phase plates (CPP)[4], and lens array (LA)[5]. Moreover, smoothing by spectral dispersion (SSD)[6], polarization smoothing (PS)[7], and multiple-beam overlap are used to suppress the amplitude of high spatial frequency within a focal spot. Excellent irradiation uniformity is achieved through two-dimensional (2D) SSD, DPP, PS, and multiple-beam overlap in OMEGA[1]. Compared with the patterns derived by phase plates, the focal spot speckle pattern obtained by LA is not completely random. The power spectra of such patterns are concentrated in certain spatial frequencies, and non-uniformity contrast is less than 100%. On the basis of numerical analysis, researchers proposed a scheme[8,9] that combines LA and SSD.

The current letter presents the experimental performance of combined one-dimensional (1D) SSD and LA technology, as applied in the ninth beam of SG-II. Using 3ω spectral dispersion with a bandwidth of 270 GHz and a line dispersion that is 24.9 times the beam's diffraction-limited width (DLW) decreases the focal spot non-uniformity of 80% energy concentration from 46% to 17%. The multiple beam interference properties of the LA are theoretically and experimentally validated by spatial power spectral density (PSD) analysis. Peak–spectra suppression ratios of 20 and 10 dB are achieved in the dispersion and orthogonal directions, respectively.

The schematic of an LA, focusing lens, and target plane in the ninth beam of SG–II is shown in Fig. 1, where the x-y plane refers to a plane transversal to the optical axis, F is the focal length of the lens, δ defines the size

of the focal spot, D is the beam aperture, and d is the sub-aperture diameter of the LA. Far-field irradiation is a temporal integral of the instantaneous laser intensity distribution at the target plane, given by[9]

$$I(x,y) = \int_0^{\Delta t} |E_{\text{FF}}(x,y,t)|^2 \mathrm{d}t, \tag{1}$$

where Δt denotes a time period that is equal to the measured laser pulse width. $E_{\text{FF}}(x,y,t)$ is the complex-valued electric field at the target plane. It is the spatial Fourier transform of $E_{\text{NF}}(x,y,t)$, the complex-valued electric field at the 3ω near field. $E_{\text{NF}}(x,y,t)$ is written as

$$E_{\text{NF}}(x,y,t) = E_0(x,y,t) \exp\left[\mathrm{i}\phi_{\text{SSD}}(x,y,t)\right] \cdot \exp\left[\mathrm{i}\phi_{\text{LA}}(x,y)\right], \tag{2}$$

where $E_0(x,y,t)$ defines the initial temporal and spatial electric field, including amplitude and phase distributions; $\phi_{\text{SSD}}(x,y,t)$ is the 1D SSD phase contribution; $\phi_{\text{LA}}(x,y)$ is the LA phase contribution.

The spatial and temporal phase contribution of 1D SSD in the dispersion direction of the x axis can be written as[1]

$$\phi_{\text{SSD}}(x,y,t) = 3\delta_x \sin\left[2\pi f_{\text{rf}}(t + \xi x)\right], \tag{3}$$

where δ_x is the 1ω laser modulation depth[10], f_{rf} denotes the modulation frequency, and ξ[1] represents a parameter related to the spectral dispersion of grating. The
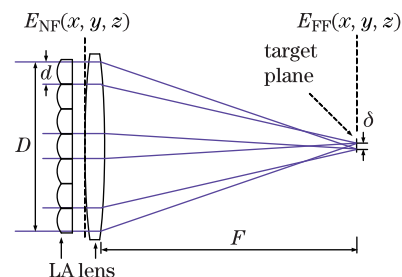

Fig. 1. Schematic of the LA, focusing lens, and target.

parameters of the 1D SSD are listed in Table 1. Two separate phase modulators are integrated in the front-end system of the ninth beam of SG-II. The first modulation frequency is 10 GHz and the second is 3 GHz. The 1ω spectral bandwidth is 0.3 nm, the corresponding 3ω bandwidth is ∼270 GHz, and the line dispersion is 24.9 times the beam's DLW. The frequency modulation to amplitude modulation conversion (FM-to-AM) induced by spatial filter is fully investigated[11]. Spectral dispersion is introduced between the Φ40 mm faraday isolator (FR40) and the third Φ40 mm rod-amplifier (403) (Fig. 2). The groove density of the grating is 1480 l/mm and the beam aperture at the grating is ∼30 mm. Thus, the spectral dispersion parameter ξ is 0.81 ns/m, with a 310 mm beam aperture at the focusing lens.

The phase contribution of a LA with N×N square apertures is given by[12]

$$\varphi_{LA}(x,y) = \sum_{m=1}^{N}\sum_{n=1}^{N} \text{rect}\left(\frac{x-x_{mn}}{d}\right)\text{rect}\left(\frac{y-y_{mn}}{d}\right)$$

$$\times \exp\left\{-i\frac{k}{2f}[(x-x_{mn})^2+(y-y_{mn})^2]\right\}, \quad (4)$$

where (x_{mn}, y_{mn}) represents the central coordinate of the sub-aperture located in row m and column n at the x-y plane, d is the sub-aperture diameter, and f is the corresponding focal length. In the experiment, d is 47.2 mm, N is 7, and f is 92.925 m.

The beam DLW is equal to the speckle size in the focal spot. The width is defined by $2.44F\lambda/D = 4.35$ μm, where F is the focal length of the lens (F=1.575 m), λ denotes the 3ω laser wavelength (λ=351 nm), and D represents the beam aperture (D=310 mm). In the measurement, the focal spot size on the target is photographed by a CCD camera at ∼12× magnification. The CCD sensor has an array of 1024×1024 elements with a pixel size of 13 μm. One pixel of the CCD camera corresponds to 1.08 μm in the target plane, a value less than a quarter of the DLW.

The measured focal spot images of 3 ns laser pulses without frequency modulation and with 1D SSD are shown in Figs. 3(a) and 3(b), respectively. The horizontal and vertical directions in Fig. 3 refer to the x and y directions in Fig. 1, respectively. The comparison of
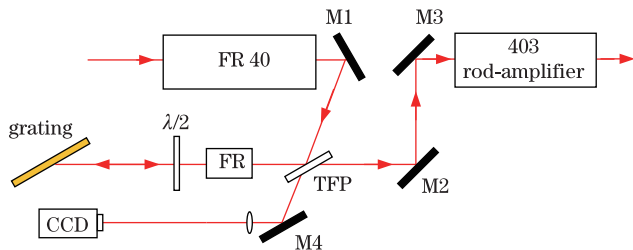
Fig. 2. Schematic of the 1D spectral dispersion.

Table 1. Spectral Dispersion Parameters for the Ninth Beam of SG-II

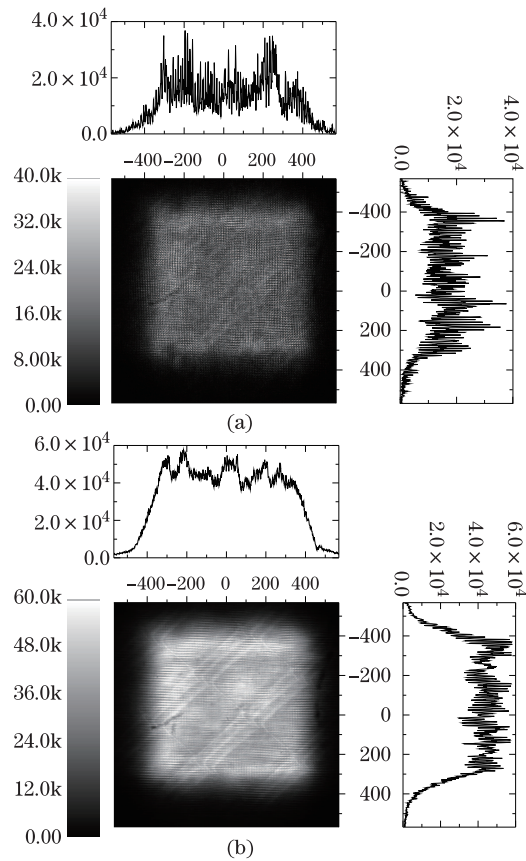| Circle Cycle	Dispersion (DLW/nm)	1ω Spectrum (nm)	ξ (ns/m)
2.49(10 GHz) 0.75(3 GHz)	83	0.3	0.81

Fig. 3. Measured focal spot images.

the 2D gray distributions illustrates that 1D SSD significantly improves irradiation uniformity. In the dispersion direction, images subjected to 1D SSD show a smooth spatial intensity envelop (see single-pixel lineout in the horizontal direction in Fig. 3(b)), whereas those exposed to pulses without frequency modulation exhibit a highly modulated spatial intensity profile (see single-pixel lineout in the horizontal direction in Fig. 3(a)). Meanwhile, the spatial intensity profile in the vertical direction is also considerably improved. Focal spot image is the overlap of a sequence of instantaneous focal spot patterns shaped by LA (refer to Eq. (1)). With spectral dispersion, each focal spot pattern is shifted in space along the horizontal direction—an approach that can also be called "beam sweeping." According to the basic concept of SSD, the irradiation uniformity of the focal spot can be improved merely by beam sweeping. Given that sweeping by 1D SSD occurs only in the dispersion (horizontal) direction, the spatial intensity profile in this direction is much smoother than that in the vertical direction.

The encircled energy fraction[2] and normalized contrast of the focal spot images are analyzed, as shown in Fig. 4, where SSD1 refers to the 3 GHz frequency modulation, and SSD2 is the 1D SSD of the combined 3 and 10 GHz frequency modulation. SSD1 and SSD2 have the same spectral bandwidth. The normalized non-uniformity contrast (RMS) of the focal spot is defined as

$$\sigma = \sqrt{\frac{1}{n}\sum_{j=1}^{n}\left(\frac{I_j-\overline{I}}{\overline{I}}\right)^2}, \quad (5)$$

where $\overline{I}$ is the average intensity of the encircled area. In Fig. 4, the thin solid black curve, thin dashed red curve, and thin dotted blue curve represent the encircled energy fractions of the focal spots without frequency modulation, with the 1D SSD of 3 GHz frequency modulation, and with the 1D SSD of the combined 3 and 10 GHz frequency modulation, respectively. These three curves are nearly overlapping, indicating that the energy concentrations of the focal spots are unaffected by the application of 1D SSD. The thick solid black curve, thick dashed red curve, and thick dotted blue curve represent the contrast of the focal spots without frequency modulation, with the 1D SSD of 3 GHz frequency modulation, and with the 1D SSD of the combined 3 and 10 GHz frequency modulation, respectively. The turning point of these three curves is around 80% of the encircled energy fraction, and the corresponding spot radius is 83.2 times the DLW. At this point, focal spot non-uniformity contrast decreases from 46% under the absence of frequency modulation to 17% under 1D SSD. Given the edge slope of the focal spots, contrast significantly increases when the calculation area is larger than 83.2 times the DLW.

The spatial PSD[1,13] is shown in Fig. 5. The thick solid black curves and thin solid red curves in Fig. 5 represent the spatial PSDs without frequency modulation and with 1D SSD (SSD1 in Fig. 4), respectively. The spatial spectral distribution is calculated by 2D Fourier transform with a hamming window applied to the focal spot data. Three different algorithms are used to analyze the spatial PSD: (1) the power spectrum is the sum at each spatial frequency in the dispersion direction (horizontal direction, Fig. 5(a)); (2) the power spectrum is the sum at each spatial frequency in the vertical direction (Fig. 5(b)); (3) the power spectrum is the azimuthal sum at each spatial frequency in a polar coordinate (Fig. 5(c)).

Without frequency modulation, five peak spectra (thick solid black curves in Figs. 5(a) and 5(b)) appear, with corresponding spatial frequencies that are 1 to 5 times the frequency of 0.079 μm^{-1}. Because the focal spot shaped by LA is a convolution of multiple beam interference patterns and Fresnel diffraction patterns[5], the focal spots have principal maxima with a spatial frequency of $d/F\lambda = 0.085$ μm^{-1} and $N\text{-}2=5$ secondary maxima between two adjacent principal maxima, where N is the number of sub-apertures. In ideal conditions, six peak spectra should appear in the spatial PSD. However, six times the spatial frequency of 0.085 μm^{-1} is a value higher than the cutoff frequency (0.46 μm^{-1}, dashed black line in Fig. 5), determined by 2 multiplied the reciprocal of the DLW. Thus, only five peak spectra are observed in the experiments. Table 2 shows that the theoretical predictions for the peak frequencies excellently agree with the experimental results.

Because the peak spectra in the horizontal direction are effectively suppressed by 1D SSD (thin solid red curve in Fig. 5(a)), the spatial PSDs in the vertical direction and in the polar coordinates (thin solid red curve in Figs. 5(b) and 5(c)) are basically the same. For the first four peak spectra, suppression ratios of 20 and 10 dB are achieved in the dispersion and orthogonal directions, respectively.
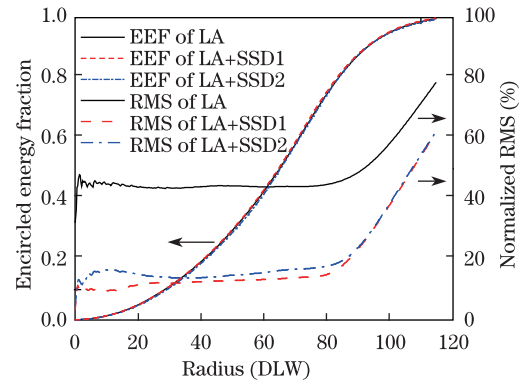

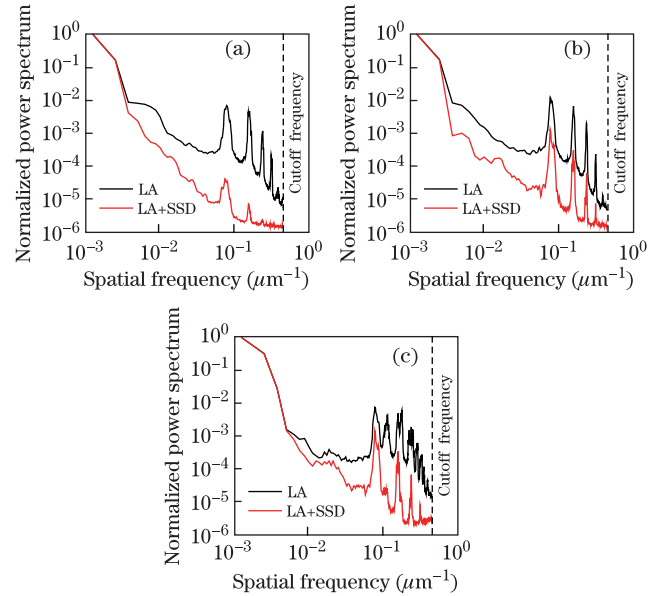Fig. 4. (Color online) Encircled energy fraction and contrast of the focal spot.

Fig. 5. (Color online) Power spectra calculated from the focal spot by using different algorithms.

Table 2. Spatial Frequencies of the Peak Spectra

Peak Frequency	1st	2nd	3rd	4th	5th
Predictions (μm^{-1})	0.085	0.170	0.255	0.340	0.425
Measurements (μm^{-1})	0.079	0.16	0.24	0.313	0.388
Difference	7.1%	5.9%	5.9%	7.9%	8.7%

Fraction power above intensity (FOPAI) refers to the ratio between the sum of laser energy higher than a certain intensity and total energy; it is defined as[2]

$$\text{FOPAI}(I_{\text{o}}) = \frac{\int_{I(x,y) \geqslant I_0} I(x,y)\mathrm{d}x\mathrm{d}y}{\int_{I(x,y)}\mathrm{d}x\mathrm{d}y}. \quad (6)$$

A steep FOPAI curve, which is close to the average intensity line, indicates excellent uniformity. In Fig. 6, the thick solid black curve is the result without frequency modulation. The thin solid blue curve and thin dotted red line show the results with the 1D SSD of 3 GHz frequency modulation and with the 1D SSD of the combined 3 and 10 GHz frequency modulation, respectively. When SSD is applied, the FOPAI curve becomes steeper,
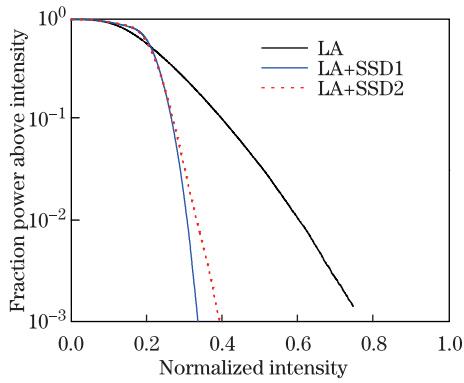
Fig. 6. (Color online) FOPAI of different experimental results.

indicating that the strong intensity area of the focal spot is effectively reduced and that uniformity significantly improves. Because the color cycle of the 10 GHz modulation is 2.49, the effect of coherence among periodic color cycles is apparent[13]. Thus, the smoothing effect of SSD2 is not as good as that of SSD1, as verified by Figs. 4 and 6.

In conclusion, the effectiveness of beam smoothing by 1D SSD and LA is verified by online experiments carried out on the ninth beam of SG-II. Using 3ω spectral dispersion with a bandwidth of 270 GHz and a line dispersion that is 24.9 times the DLW decreases the normalized focal spot non-uniformity of 80% energy concentration from 46% to 17%. The encircled energy fraction is unaffected by 1D SSD. For the first four peak spectra, suppression ratios of 20 and 10 dB are achieved in the dispersion and orthogonal directions, respectively. Thus, the peak spectra caused by multiple beam interference of the LA are effectively reduced by 1D SSD. Furthermore, if another orthogonal-direction SSD is incorporated into the smoothing process, higher uniformity can be expected.

References

1. S. P. Regan, J. A. Marozas, R. S. Craxton, J. H. Kelly, W. R. Donaldson, P. A. Jaanimagi, D. J. Perkins, R. L. Keck, T. J. Kessler, D. D. Meyerhofer, T. G. Sangster, W. Seka, V. A. Smalyuk, S. Skupsky, and J. D. Zuegel, J. Opt. Soc. Am. B **22,** 998 (2005).
2. C. A. Haynam, P. J. Wegner, J. M. Auerbach, M. W. Bowers, S. N. Dixit, G. V. Erbert, G. M. Heestand, M. A. Henesian, M. R. Hermann, K. S. Jancaitis, K. R. Manes, C. D. Marshall, N. C. Mehta, J. Menapace, E. Moses, J. R. Murray, M. C. Nostrand, C. D. Orth, R. Patterson, R. A. Sacks, M. J. Shaw, M. Spaeth, S. B. Sutton, W. H. Williams, C. C. Widmayer, R. K. White, S. T. Yang, and B. M. Van Wonterghem, Appl. Opt. **46,** 3276 (2007).
3. Y. Lin, T. J. Kessler, and G. N. Lawrence, Opt. Lett. **20,** 764 (1995).
4. Y. Arieli, Opt. Commun. **180,** 239 (2000).
5. X. M. Deng, X. C. Liang, Z. Z. chen, W. Y. Yu, and R. Y. Ma, Appl. Opt. **25,** 377 (1986).
6. S. Skupsky, R. W. Short, T. Kessler, R. S. Craxton, S. Letzring, and J. M. Soures, J. Appl. Phys. **66,** 3456 (1989).
7. J. E. Rothenberg, J. Appl. Phys. **87,** 3654 (2000).
8. S. L. Zhou and Z. Q. Lin, Acta Opt. Sin. **27,** 275 (2007).
9. X. J. Jiang, S. L. Zhou, and Z. Q. Lin, J. Appl. Phys. **101,** 023109 (2007).
10. Y. Jiang, X. Li, S. Zhou, W. Fan, and Z. Lin, Chin. Opt. Lett. **11,** 052301 (2013).
11. H. Zhang, S. Zhou, Y. Jiang, J. Li, W. Feng, and Z. Lin, Chin. Opt. Lett. **10,** 060501 (2012).
12. Y. Qiu, L. J. Qian, H. Y. Huang, D. Y. Fan, and X. M. Deng, Chinese J. Lasers **22,** 27 (1995).
13. J. E. Rothenberg, J. Opt. Soc. Am. B **14,** 1664 (1997).